

A Bayesian Statistical Method for the Detection and Quantification of Rotational Diffusion Anisotropy from NMR Relaxation Data

Michael Andrec,*† Keith G. Inman,‡ David J. Weber,‡ Ronald M. Levy,†¹ and Gaetano T. Montelione*‡²

*Center for Advanced Biotechnology and Medicine, †Department of Chemistry, Wright-Rieman Laboratories, and ‡Department of Molecular Biology and Biochemistry, Rutgers, The State University of New Jersey, Piscataway, New Jersey 08855-0939; and ‡Department of Biological Chemistry, University of Maryland School of Medicine, Baltimore, Maryland 21201

Received December 7, 1999; revised April 20, 2000

It has recently become more widely appreciated that the presence of rotational diffusional anisotropy in proteins and other macromolecules can have a significant affect on the interpretation of NMR relaxation data in terms of molecular motion. In this paper, we show how commonly used NMR relaxation data (R_1 , R_2 , and NOE) obtained at two spectrometer frequencies can be analyzed using a Bayesian statistical approach to reliably detect and quantify the degree of rotational diffusion anisotropy. Our approach differs from previous methods in that it does not make assumptions concerning the internal motions experienced by the residues which are used to quantify the diffusion anisotropy, but rather averages the results over all internal motions consistent with the data. We demonstrate our method using synthetic data corresponding to isotropic, axially symmetric anisotropic, and fully asymmetric anisotropic rotational diffusion, as well as experimental NMR data. We compare the Bayesian statistical approach with a widely used method for extracting tumbling parameters using both synthetic and experimental data. While it can be difficult to separate the effects of chemical exchange from rotational anisotropy using this "standard" method, these effects are readily separated using Bayesian statistics. In addition, we find that the Bayesian statistical approach requires considerably less CPU time than an equivalent standard analysis. © 2000 Academic Press

Key Words: backbone dynamics; Lipari–Szabo formalism; rotational correlation time; Monte Carlo; multiple fields; chemical exchange.

INTRODUCTION

It is well known that NMR is a powerful tool for the study of internal motions in macromolecules (1, 2). However, interpretation of such data in terms of internal motions is contingent upon the accurate description of the overall tumbling of the molecule in solution (3, 4). It has recently become more widely appreciated that the neglect of rotational diffusional anisotropy can result in potentially serious misinterpretation of the NMR relaxation data in terms of molecular motion (3, 5). For exam-

ple, given a protein whose shape can be well approximated by a prolate ellipsoid, bond vectors parallel to the long axis will display significantly faster transverse relaxation rates (R_2) than those perpendicular to the long axis. If one incorrectly assumes that a protein is spherical, then the estimate of the overall correlation time could be dominated by a relatively large number of bond vectors oriented perpendicular to the symmetry axis, and one might erroneously attribute a contribution to R_2 from chemical exchange (R_{ex}) for those oriented along the symmetry axis (3, 6).

Methods which estimate the overall tumbling parameters from the ratio of the transverse and longitudinal relaxation rates (R_2/R_1) must somehow eliminate from consideration all residues which in fact *do* have significant contributions from chemical exchange processes, as their inclusion would cause systematic error in the resulting parameter values. One commonly used method for achieving this selection is to remove residues which satisfy the criterion

$$\frac{\langle T_2 \rangle - T_{2,n}}{\langle T_2 \rangle} - \frac{\langle T_1 \rangle - T_{1,n}}{\langle T_1 \rangle} > 1.5 \text{ SD}, \quad [1]$$

where $T_{1,n}$ and $T_{2,n}$ are the longitudinal and transverse relaxation time constants for residue n , the means are taken over all residues for which the steady-state heteronuclear NOE is greater than 0.65, and SD represents the standard deviation of the left-hand side of Eq. [1] over all residues (NOE > 0.65) (7, 8). Clearly, this criterion makes assumptions about the distribution of internal motions in the protein (e.g., that most residues in the molecule do not have R_{ex} contributions). The analysis is further complicated by the possible attribution of R_{ex} contributions to residues which in fact are not undergoing chemical exchange but have orientations very close to the major diffusion axis (6). Separation of anisotropy and chemical exchange effects using rotating frame relaxation dispersion (9–11), cross-correlated relaxation (12), or residual dipolar couplings (6) has been proposed; however, these methods require the implementation of additional experimental methods beyond the measurement of R_1 , R_2 , and heteronuclear NOE. Such methods can be experimentally challenging and can be

¹ To whom correspondence should be addressed. Fax: (732) 445-5958. E-mail: ronlevy@lutece.rutgers.edu.

² To whom correspondence should be addressed. Fax: (732) 235-4850. E-mail: guy@nmrlab.cabm.rutgers.edu.

prone to additional systematic errors beyond those inherent in the traditional set of relaxation experiments. One could also detect R_{ex} contributions via their quadratic dependence on the spectrometer field strength, and several laboratories have tried to make use of this information (8, 13, 14). Our approach makes use of a general statistical formalism within which it is possible to combine relaxation data obtained at multiple spectrometer fields (or other sources) and the effects of rotational anisotropy and chemical exchange can be separated.

Rather than reducing the amount of data used in the estimation of overall tumbling by neglecting residues which may potentially have τ_e or R_{ex} contributions, it is possible to make use of all of the relaxation data, while at the same time avoiding unnecessary assumptions concerning the internal motion experienced by any given residue. As we have described previously, such information can be usefully summarized in the form of a Bayesian marginal posterior probability density function (4). In this paper, we show how these marginal densities for the apparent rotational correlation time $\tau_{\text{m,app}}^{(i)}$ constructed using R_1 , R_2 , and NOE data collected at two spectrometer field strengths can be used to detect, quantify, and assess the statistical significance of rotational diffusion anisotropy in macromolecules.

THEORY

We consider ^1H - ^{15}N internuclear vectors whose internal motions can be described by the Lipari-Szabo ‘‘model-free’’ formalism (15), in which the spectral density is given by

$$J(\omega) = \frac{2}{5} \left[\frac{S^2 \tau_{\text{m}}}{1 + \omega^2 \tau_{\text{m}}^2} + \frac{(1 - S^2) \tau}{1 + \omega^2 \tau^2} \right], \quad [2]$$

where S^2 is a measure of the spatial restriction of the internal motion, τ_e is a measure of the timescale of the internal motion, τ_{m} is the rotational correlation time for the overall isotropic tumbling, and $\tau^{-1} = \tau_e^{-1} + \tau_{\text{m}}^{-1}$. In addition, we model the effect of chemical exchange as $R_{\text{ex}} = \omega_{\text{N}}^2 \Phi_{\text{ex}}$, where ω_{N} is the Larmor frequency of ^{15}N and Φ_{ex} is a constant that depends on the chemical shift differences, populations, and interconversion rates for the exchanging species (2).

Consider a set of bond vectors embedded in an ellipsoid undergoing rotational diffusion with $D_{xx} \leq D_{yy} \leq D_{zz}$, where D_{ii} is the diffusion coefficient for reorientation about the i th axis of the principal axis system (PAS) of the molecule. Note that in our convention, D_{zz} is the largest of the diffusion coefficients, and is unrelated to any symmetry which may be present. If we fit the adjustable parameters of Eq. [2] to the relaxation data for each bond vector while allowing τ_{m} to vary independently, then the resulting apparent τ_{m} values $\tau_{\text{m,app}}^{(i)}$ for all residues i are approximately determined by the D_{ii} ’s and the orientation of the i th bond vector in the PAS (3, 7, 16). In order to make use of this information for the analysis of dynamics, one must know the relative orientations of all of the bond

vectors for which there are relaxation data, which must be obtained from a high-resolution NMR or X-ray crystal structure.

Two different approximate expressions for $\tau_{\text{m,app}}^{(i)}$ in terms of the diffusion coefficients and orientation have been proposed. The first, proposed by Schurr, Babcock, and Fujimoto (3) (SBF), assumes that the ellipsoid is axially symmetric (i.e., $D_{zz} = D_{\parallel} \geq D_{xx} = D_{yy} = D_{\perp}$ (prolate), or $D_{zz} = D_{yy} = D_{\perp} \geq D_{xx} = D_{\parallel}$ (oblate)). In this case, the bond vector orientation for residue i is given by the angle θ_i of the bond vector relative to the D_{\parallel} axis. The SBF approximation is then given by

$$\tau_{\text{m,app}}^{(i)} = \frac{\frac{1}{4}(3 \cos^2 \theta_i - 1)^2}{6D_{\perp}} + \frac{3 \cos^2 \theta_i \sin^2 \theta_i}{5D_{\perp} + D_{\parallel}} + \frac{\frac{3}{4} \sin^4 \theta_i}{2D_{\perp} + 4D_{\parallel}}. \quad [3]$$

The latter, proposed by Brüsweiler, Liao, and Wright (16) (BLW), does not assume axial symmetry, but is valid only for ‘‘small’’ anisotropies. It is given by

$$(6\tau_{\text{m,app}}^{(i)})^{-1} = Q_{xx}x_i^2 + Q_{yy}y_i^2 + Q_{zz}z_i^2, \quad [4]$$

where x_i , y_i , and z_i are the direction cosines of the internuclear vector i relative to the PAS and Q_{ii} is the diffusion coefficient for the motion of the i th axis of the PAS and is given by $Q_{xx} = (D_{yy} + D_{zz})/2$, $Q_{yy} = (D_{xx} + D_{zz})/2$, and $Q_{zz} = (D_{xx} + D_{yy})/2$ (17).

As we have described previously (4), given a set of j ($j = 1, \dots, n$) NMR relaxation measurements R_{ij} for each of the i ($i = 1, \dots, N$) residues one can construct the joint posterior probability density for the model parameters. In the following, R_{ij} will represent a given relaxation measurement j (e.g., R_1 , R_2 , or NOE) for a given residue i , R_i will represent the complete vector of relaxation measurements for residue i , and R will represent the complete set of relaxation data for all residues. The local posterior probability density for residue i is constructed by applying the Bayes theorem to the likelihood of the data and the prior probability of the parameters (18),

$$P(S^2, \tau_e, R_{\text{ex}}, \tau_{\text{m,app}}^{(i)} | R_i) = \frac{P(R_i | S^2, \tau_e, R_{\text{ex}}, \tau_{\text{m,app}}^{(i)}) P(S^2, \tau_e, R_{\text{ex}}, \tau_{\text{m,app}}^{(i)})}{P(R_i)}, \quad [5]$$

where $P(R_i)$ is a normalization constant. The likelihood of observing the data R_i given that the underlying dynamic processes are described by the given values of S^2 , τ_e , R_{ex} , and $\tau_{\text{m,app}}^{(i)}$ is taken to be

$$P(R_i|S^2, \tau_e, R_{ex}, \tau_{m,app}^{(i)}) = \prod_{j=1}^n \frac{1}{\sqrt{2\pi\sigma_{ij}^2}} \exp\left[-\frac{(R_{ij} - R_{ij}^{(calc)})^2}{2\sigma_{ij}^2}\right], \quad [6]$$

$$R_{axial} = \begin{cases} \frac{2D_{zz}}{D_{xx} + D_{yy}}, & D_{zz}/D_{yy} > D_{yy}/D_{xx} \text{ (prolate-like)} \\ \frac{2D_{xx}}{D_{yy} + D_{zz}}, & D_{zz}/D_{yy} < D_{yy}/D_{xx} \text{ (oblate-like)} \end{cases}. \quad [8]$$

where $R_{ij}^{(calc)}$ is the j th relaxation parameter calculated using the given values of S^2 , τ_e , R_{ex} , and $\tau_{m,app}^{(i)}$, and σ_{ij} is the uncertainty in the j th observed relaxation value for the i th residue. The prior probability $P(S^2, \tau_e, R_{ex}, \tau_{m,app}^{(i)})$ is taken to be equal to one in the region $0 < S^2 < 1$, $\tau_e \geq 0$, $R_{ex} \geq 0$, $\tau_{m,app}^{(i)} > 0$, and zero outside of this region. We can summarize the information content regarding $\tau_{m,app}^{(i)}$ in the data R_i by means of the marginal posterior probability density of $\tau_{m,app}^{(i)}$:

$$P(\tau_{m,app}^{(i)}|R_i) = \int P(S^2, \tau_e, R_{ex}, \tau_{m,app}^{(i)}|R_i) dS^2 d\tau_e dR_{ex}. \quad [7]$$

The marginal density $P(\tau_{m,app}^{(i)}|R_i)$ can be thought of as the knowledge that we have about the value of $\tau_{m,app}^{(i)}$ averaged over all possible internal motions (values of S^2 , τ_e , and R_{ex}) weighted by their consistency with the data. Although the integral in Eq. [7] cannot be solved in closed form, it is nonetheless quite straightforward to generate a Monte Carlo sample of points distributed according to $P(S^2, \tau_e, R_{ex}, \tau_{m,app}^{(i)}|R_i)$, from which a numerical approximation to the function $P(\tau_{m,app}^{(i)}|R_i)$ can be generated (see Appendix B) (4). It is clear that at least four relaxation data must be included in R_i for the marginal density $P(\tau_{m,app}^{(i)}|R_i)$ to be informative, since otherwise the parameter estimation problem is underdetermined. Thus, the traditional R_1 , R_2 , and NOE measurements at one field strength must be supplemented with additional data, either by repeating the measurements at a different field strength or by including cross-correlated relaxation data (4).

For the general case of fully asymmetric anisotropic tumbling, the diffusion tensor can be described by six parameters: the three principle values D_{xx} , D_{yy} , and D_{zz} and the three Euler angles ϕ , θ , and χ describing the orientation of the PAS relative to an arbitrarily chosen molecular reference frame. On the other hand, for axially symmetric tumbling, the diffusion tensor is usually described by the four parameters D_{\parallel} , D_{\perp} , ϕ , and θ , where D_{\parallel} and D_{\perp} were defined in Eq. [3] above, and ϕ and θ give the orientation of the symmetry axis in the molecular frame. In order to more easily compare results for axially symmetric and fully anisotropic fits and to be able to more easily constrain the BLW approximation to axial symmetry, it is convenient to introduce the following parameters: D_{iso} , R_{axial} , and R_{asym} . D_{iso} is the magnitude of the isotropic portion of the diffusion tensor and is given by $(D_{xx} + D_{yy} + D_{zz})/3$ or $(2D_{\perp} + D_{\parallel})/3$. The parameter R_{axial} describes the degree of axially symmetric anisotropy; it has values less than 1 for oblate ellipsoids and greater than 1 for prolate ellipsoids. For axially symmetric tumbling, R_{axial} is simply equal to D_{\parallel}/D_{\perp} . For the BLW approximation, we define it to be

The parameter R_{asym} describes the degree of deviation from axial symmetry, and is defined to be

$$R_{asym} = \begin{cases} \frac{D_{xx}}{D_{yy}}, & D_{zz}/D_{yy} > D_{yy}/D_{xx} \text{ (prolate-like)} \\ \frac{D_{yy}}{D_{zz}}, & D_{zz}/D_{yy} < D_{yy}/D_{xx} \text{ (oblate-like)} \end{cases}. \quad [9]$$

R_{asym} is obviously equal to 1 for axially symmetric tumbling.

Given an orientation for each $^1\text{H}-^{15}\text{N}$ internuclear vector i in an arbitrarily chosen molecular frame (e.g., the coordinate system of a PDB file), we can use Eq. [3] or [4] to calculate the expected $\tau_{m,app}^{(i)}$ value for that vector as a function of the six tensor parameters: $\tau_{m,app}^{(i)}(D_{iso}, R_{axial}, R_{asym}, \phi, \theta, \chi)$. It should be emphasized that the angles ϕ , θ , and χ relate the orientation of the PAS to the molecular frame, and do not represent orientations of individual bond vectors i . We can then evaluate the probability of a point in the tensor parameter space by taking the product of the marginal probability densities over all N residues evaluated at their respective expected $\tau_{m,app}^{(i)}$ values. Under the assumptions of isotropic, axially symmetric anisotropic, and fully asymmetric anisotropic tumbling, respectively, the posterior probabilities are given by

$$P_{iso}(D_{iso}|R) = \prod_{i=1}^N P(\tau_{m,app}^{(i)}(D_{iso}, R_{axial} = 1, R_{asym} = 1)|R_i) \times P_{iso}(D_{iso})/P_{iso}(R), \quad [10a]$$

$$P_{axial}(D_{iso}, R_{axial}, \phi, \theta, \chi|R) = \prod_{i=1}^N P(\tau_{m,app}^{(i)}(D_{iso}, R_{axial}, R_{asym} = 1, \phi, \theta, \chi)|R_i) \times P_{axial}(D_{iso}, R_{axial}, \phi, \theta, \chi)/P_{axial}(R), \quad [10b]$$

and

$$P_{asym}(D_{iso}, R_{axial}, R_{asym}, \phi, \theta, \chi|R) = \prod_{i=1}^N P(\tau_{m,app}^{(i)}(D_{iso}, R_{axial}, R_{asym}, \phi, \theta, \chi)|R_i) \times P_{asym}(D_{iso}, R_{axial}, R_{asym}, \phi, \theta, \chi)/P_{asym}(R), \quad [10c]$$

where R represents the relaxation data for all N residues, $P_{iso}(D_{iso})$, $P_{axial}(D_{iso}, R_{axial}, \phi, \theta, \chi)$, and $P_{asym}(D_{iso}, R_{axial}, R_{asym})$.

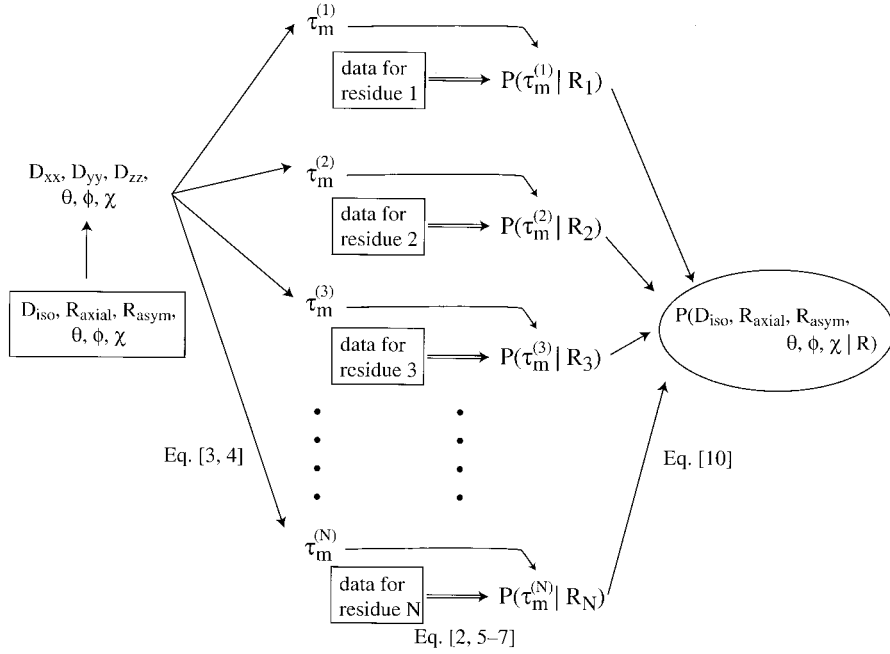


FIG. 1. A schematic representation of the information flow in the calculation of the posterior probability of a point in tensor parameter space.

ϕ , θ , χ) are the prior probabilities over the tensor parameters, and $P_{\text{iso}}(R)$, $P_{\text{axial}}(R)$, and $P_{\text{asym}}(R)$ are normalization constants which represent the relative probabilities of the three different tumbling models (see below). Equation [10a] is, of course, equivalent to directly taking the product over all residues of the marginal densities for the apparent tumbling correlation time $\tau_{\text{m,app}}^{(i)}$, as described previously (4). A graphical representation of Eq. [10] and the overall organization of the probability densities are shown in Fig. 1. It should be noted that for our parameterization, it is necessary in Eq. [10b] to allow all three Euler angles to vary when $R_{\text{axial}} = 1$, even though there are only two angular degrees of freedom. This is because in that case, rotations about the symmetry axis (the x axis of the PAS) correspond to a nontrivial function of ϕ , θ , and χ . For purposes of this study, we define the priors $P_{\text{axial}}(D_{\text{iso}}, R_{\text{axial}}, \phi, \theta)$, and $P_{\text{asym}}(D_{\text{iso}}, R_{\text{axial}}, R_{\text{asym}}, \phi, \theta, \chi)$ to be

$$P_{\text{axial}}(D_{\text{iso}}, R_{\text{axial}}, \phi, \theta) = P_{\text{iso}}(D_{\text{iso}}) P_{\text{axial}}(R_{\text{axial}}) P(\phi) P(\theta) \quad [11a]$$

and

$$P_{\text{asym}}(D_{\text{iso}}, R_{\text{axial}}, R_{\text{asym}}, \phi, \theta, \chi) = P_{\text{iso}}(D_{\text{iso}}) P_{\text{asym}}(R_{\text{axial}}, R_{\text{asym}}) P(\phi) P(\theta) P(\chi), \quad [11b]$$

where the priors $P_{\text{iso}}(D_{\text{iso}})$, $P(\phi)$, $P(\theta)$, and $P(\chi)$ are taken to be independent and uniform inside the regions $D_{\text{iso}} > 0$, $0^\circ \leq \phi \leq 360^\circ$, $0^\circ \leq \theta \leq 180^\circ$, and $0^\circ \leq \chi \leq 360^\circ$, and equal to

zero outside of those regions. The construction of $P_{\text{axial}}(R_{\text{axial}})$ and $P_{\text{asym}}(R_{\text{axial}}, R_{\text{asym}})$ is described in detail in Appendix A.

COMPUTATIONAL METHODS

Three synthetic data sets corresponding to R_1 , R_2 , and NOE data at spectrometer frequencies of 400 and 600 MHz for 30 residues were generated using a variety of realistic local dynamic parameters (including $R_{\text{ex}} \neq 0$) (Table 1) and three diffusion tensors: isotropic, axially symmetric anisotropic, and fully asymmetric anisotropic (Table 2). The isotropic case serves as a reference as well as a test of the methodology to distinguish isotropic tumbling in the presence of chemical exchange from anisotropic tumbling. The data were generated using the spectral density function for the Lipari–Szabo formalism in the presence of fully asymmetric anisotropic tumbling,

$$J(\omega) = \frac{2}{5} \left[S^2 \sum_{k=1}^5 \frac{A_k \tau_k}{1 + \omega^2 \tau_k^2} + \frac{(1 - S^2) \tau}{1 + \omega^2 \tau^2} \right], \quad [12]$$

where $A_1 = 3y^2z^2$, $A_2 = 3x^2z^2$, $A_3 = 3x^2y^2$, $A_4 = d - e$, $A_5 = d + e$, $d = \frac{1}{4}[3(x^4 + y^4 + z^4) - 1]$, $e = \frac{1}{12}[\delta_x(3x^4 + 6y^2z^2 - 1) + \delta_y(3y^4 + 6x^2z^2 - 1) + \delta_z(3z^4 + 6x^2y^2 - 1)]$, $\delta_i = (D_{ii} - D_{\text{iso}})/\sqrt{D_{\text{iso}}^2 - L^2}$, $L^2 = \frac{1}{3}(D_{xx}D_{yy} + D_{xx}D_{zz} + D_{yy}D_{zz})$, $\tau_1^{-1} = 4D_{xx} + D_{yy} + D_{zz}$, $\tau_2^{-1} = D_{xx} + 4D_{yy} + D_{zz}$, $\tau_3^{-1} = D_{xx} + D_{yy} + 4D_{zz}$, $\tau_4^{-1} = 6(D_{\text{iso}} + \sqrt{D_{\text{iso}}^2 - L^2})$, $\tau_5^{-1} = 6(D_{\text{iso}} - \sqrt{D_{\text{iso}}^2 - L^2})$, $\tau^{-1} = 6D_{\text{iso}} + \tau_c^{-1}$, and x , y , and z are the direction cosines of the bond vector

TABLE 1
Internal Motional Parameters and Orientations
Used to Generate Synthetic Data

Residue	S^2	τ_e (ps)	R_{ex} (s^{-1} at 400 MHz)	Orientation in molecular frame	
				θ (degrees)	ϕ (degrees)
1	0.90	10.0	0	160	30
2	0.88	20.0	0	100	140
3	0.86	100.0	1.92	44	12
4	0.89	250.0	0	62	280
5	0.90	30.0	0	66	240
6	0.80	5.0	1.28	100	279
7	0.94	300.0	0	74	170
8	0.75	700.0	1.60	94	140
9	0.87	350.0	0	67	334
10	0.85	200.0	2.24	103	173
11	0.91	55.0	2.69	152	176
12	0.86	150.0	0	71	71
13	0.88	600.0	0	94	356
14	0.85	3.0	0	123	133
15	0.91	250.0	0	77	90
16	0.87	2.0	1.98	133	297
17	0.94	175.0	0	140	326
18	0.88	30.0	3.39	119	154
19	0.87	3.0	0	28	101
20	0.89	25.0	1.79	30	224
21	0.88	8.0	0.77	71	224
22	0.85	520.0	2.75	99	328
23	0.89	9.0	0	103	174
24	0.90	150.0	0	125	87
25	0.86	73.0	0	61	126
26	0.90	94.0	0	135	263
27	0.87	8.0	0	56	298
28	0.80	94.0	2.05	63	157
29	0.86	472.0	1.79	107	123
30	0.88	12.0	0	80	258

in the PAS (8, 17, 19). The standard expressions for R_1 , R_2 , and NOE as a function of $J(\omega)$ (2, 20) were used to evaluate the relaxation rates. The form of the Lipari–Szabo formalism given in Eq. [12] is valid only in the limit that τ_e is at least one order of magnitude faster than any of the rotational correlation times τ_i ($i = 1, \dots, 5$) (7). This condition is satisfied by the parameters used in this study. The uncertainties σ_{ij} in Eq. [6] were taken to be 5% of the corresponding R_1 , R_2 , or NOE measurement. For demonstration purposes, we have used a uniform value of -160 ppm for the magnitude of the ^{15}N chemical shift anisotropy (CSA) for generating and analyzing the synthetic data used in this study, and it was assumed that the CSA tensor was oriented with its symmetry axis parallel to the $^{15}\text{N}-^1\text{H}$ bond vector, even though the case may be more complicated in real proteins (21–23).

A total of 19,500 Monte Carlo samples distributed according to the density $P(S^2, \tau_e, R_{ex}, \tau_{m,app}^{(i)}|R_i)$ were generated for each residue as described in detail in Appendix B. For each tensor, three sets of Monte Carlo samples consisting of 39,876 points

each were generated: the first was distributed according to $P_{axial}(D_{iso}, R_{axial}, \phi, \theta, \chi|R)$ calculated using Eqs. [3] and [10b] (the SBF approximation), the second was distributed according to $P_{axial}(D_{iso}, R_{axial}, \phi, \theta, \chi|R)$ calculated using Eqs. [4] and [10b] (the axially symmetric BLW approximation), and the third was distributed according to $P_{asym}(D_{iso}, R_{axial}, R_{asym}, \phi, \theta, \chi|R)$ using Eqs. [4] and [10c] (the fully asymmetric BLW approximation). Approximately 1 min of CPU time was required per residue for the $P(S^2, \tau_e, R_{ex}, \tau_{m,app}^{(i)}|R_i)$ Monte Carlo samples, and each tensor parameter estimation Monte Carlo run required approximately 10 min of CPU time. All calculations were performed on a Silicon Graphics R10000 computer running at 194 MHz.

RESULTS

1. Tensor Parameter Estimation

As was discussed in the Introduction, one of the challenges in the analysis of NMR relaxation data is the separation of the effects of anisotropy and chemical exchange without resorting to independent experimental methods. For Tensor 2, the symmetry axis is oriented at $(\theta, \phi) = (30^\circ, 10^\circ)$ in spherical coordinates with respect to the molecular frame (Table 2). Given that symmetry axis orientation and the spherical coordinates of the bond vectors for residues 3 and 5 in Table 1, it follows that residue 3 is located at an angle of 14° relative to the symmetry axis of Tensor 2, while residue 5 is nearly perpendicular to that axis (87°). Therefore, even if residue 3 did not have an R_{ex} contribution, its R_2 would be significantly larger than that of residue 5, and it could be difficult to determine whether the increased R_2 was due to anisotropy, chemical exchange, or both. The calculations based on simulated R_1 , R_2 , and NOE data at two field strengths allow us to evaluate the utility of the marginal densities $P(\tau_{m,app}^{(i)}|R_i)$ for disentangling the effects of anisotropy and chemical exchange. Figure 2 shows a projection of the Monte Carlo samples from $P(S^2, \tau_e, R_{ex}, \tau_{m,app}^{(3)}|R_3)$ and $P(S^2, \tau_e, R_{ex}, \tau_{m,app}^{(5)}|R_5)$ onto the $(R_{ex}, \tau_{m,app}^{(i)})$ plane, as well as a plot of the marginal densities $P(\tau_{m,app}^{(3)}|R_3)$ and $P(\tau_{m,app}^{(5)}|R_5)$. Although the estimates of $\tau_{m,app}^{(i)}$

TABLE 2
Tensor Parameters Used to Generate Synthetic Data^a

	D_{xx} (μs^{-1})	D_{yy} (μs^{-1})	D_{zz} (μs^{-1})	D_{iso} (μs^{-1}) ^b	R_{axial} ^c	R_{asym} ^d
Tensor 1	14.0	14.0	14.0	14.0	1.0	1.0
Tensor 2	14.0	14.0	25.0	17.7	1.8	1.0
Tensor 3	9.8	14.0	25.0	16.3	2.1	0.7

^a The orientation of the PAS in the molecular frame of Table 1 is given by the Euler angles $\theta = 30^\circ$, $\phi = 10^\circ$, $\chi = 50^\circ$.

^b Isotropic portion of the diffusion tensor, defined in text above Eq. [8].

^c Axially symmetric anisotropic portion of the diffusion tensor, defined in Eq. [8].

^d Asymmetry ratio of the diffusion tensor, defined in Eq. [9].

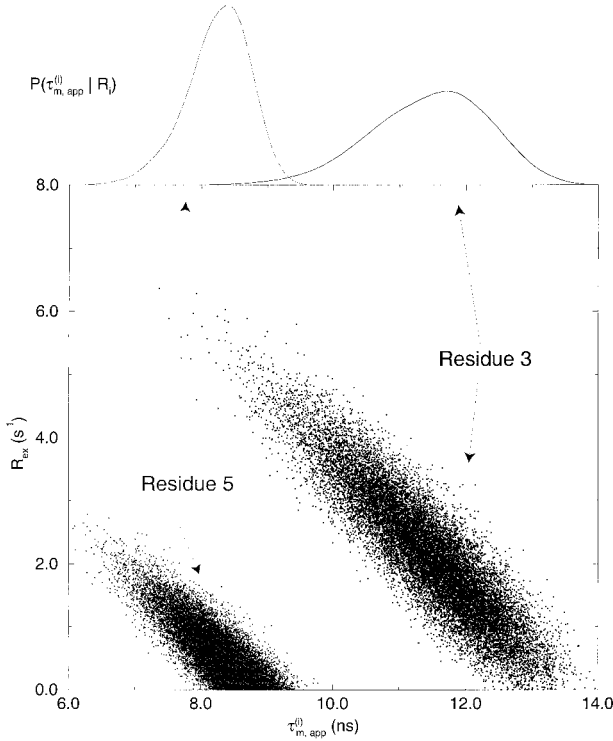


FIG. 2. Monte Carlo samples generated from the local posterior probability density $P(S^2, \tau_e, R_{ex}, \tau_{m,app}^{(i)}|R_i)$ for residues 3 and 5 projected onto the $(R_{ex}, \tau_{m,app}^{(i)})$ plane, along with the marginal posterior densities $P(\tau_{m,app}^{(3)}|R_3)$ and $P(\tau_{m,app}^{(5)}|R_5)$. The minimal overlap between the latter two curves indicates that the differences in the relaxation data for residues 3 and 5 are due at least in part to anisotropy effects, irrespective of any differences in internal motions.

and R_{ex} are strongly correlated, and lack of knowledge of the magnitude of R_{ex} substantially increases the width of the $P(\tau_{m,app}^{(i)}|R_i)$ distributions, nonetheless there is minimal overlap between the marginal densities for the apparent tumbling correlation time $P(\tau_{m,app}^{(3)}|R_3)$ and $P(\tau_{m,app}^{(5)}|R_5)$ for these two residues. This indicates that there is a significant difference in their $\tau_{m,app}^{(i)}$ values due to orientational effects associated with diffusional anisotropy and that the increased transverse relaxation rate for residue 5 cannot be explained by R_{ex} effects alone. For example, it is apparent from Fig. 2 that all values of $\tau_{m,app}^{(i)}$ having appreciable posterior probability are smaller than the value of $\tau_{m,app}^{(5)}$ even when R_{ex} is constrained to be zero. We conclude that by using the marginal densities for the local tumbling parameter $\tau_{m,app}^{(i)}$, it is possible to separate the effects of chemical exchange and anisotropy.

The marginal $\tau_{m,app}^{(i)}$ densities can be used to estimate the diffusion tensor parameters and assess the statistical significance of different models for the overall tumbling of the protein. This is done by using $P(\tau_{m,app}^{(i)}|R_i)$ together with the SBF or BLW approximations (Eqs. [3] and [4]) to generate Monte Carlo samples from the posterior probabilities of the diffusion tensor parameters $P(D_{iso}|R)$, $P_{axial}(D_{iso}, R_{axial}, \phi, \theta, \chi|R)$, and $P_{asym}(D_{iso}, R_{axial}, R_{asym}, \phi, \theta, \chi|R)$ as described above. The results of these calculations are summarized in the form of means and standard deviations of the Monte Carlo

samples (Table 3) and one-dimensional marginal densities of the tensor parameters as shown in Figs. 3 and 4. As seen in Table 3, all three estimation methods (SBF, BLW with $R_{asym} = 1$, and BLW with $R_{asym} \neq 1$) were successful in deriving the correct diffusion tensor axial asymmetry ratio and orientation from the synthetic 400- and 600-MHz R_1 , R_2 , and NOE data for both the isotropic Tensor 1 and the axially symmetric Tensor 2. Unlike the results for Tensors 1 and 2, the SBF and BLW(axial) approximations were inaccurate in their estimates of the angle θ for the fully asymmetric Tensor 3. This is not unreasonable, since an axially symmetric model is incorrect for this data set. On the other hand, the BLW(asym) method does provide accurate estimates of these parameters for Tensor 3, as well as accurate estimates of R_{asym} and χ .

As indicated in Table 3, the Monte Carlo sample for BLW(asym) exhibits bimodality, with one mode corresponding to $R_{axial} > 1$ and another with $R_{axial} < 1$ (Fig. 5). It should be noted that although these two modes are far apart in $(D_{iso}, R_{axial}, R_{asym})$ space, they are in fact contiguous in (D_{xx}, D_{yy}, D_{zz}) space, and the bimodality arises from the choice of parametrization used in this analysis. Furthermore, as the diffusion tensor becomes more asymmetric, the parameter R_{axial} has less physical meaning, since it makes less sense to describe such a tensor as prolate or oblate. However, this in no way invalidates the use of the $(D_{iso}, R_{axial}, R_{asym})$ parametrization as a computational device. Recent work by Blackledge *et al.* (24) has suggested that the fitting of a fully anisotropic diffusion tensor by an axially symmetric one can result in the sum of squared residual surfaces with multiple minima (or equivalently, multimodal likelihood functions). This bimodality arises from the (mis)fitting of an axially symmetric tensor to a fully anisotropic tensor using either the major or minor axis of the latter as the symmetry axis of the former, and is unrelated to the (R_{axial}, R_{asym}) bimodality described above. We do, however, also observe a second mode located at $D_{iso} = 17 \mu s^{-1}$ and $R_{axial} = 0.6$ when fitting Tensor 3 data with the SBF and BLW(axial) approximations. The maximum posterior probabilities of those modes are a factor of 3000 smaller than the maximum posterior probability of the modes listed in Table 3, and we conclude that the probability mass contained in those modes is negligible for these synthetic data.

It is interesting to note that for these synthetic data sets the expectation values of D_{iso} are overestimated (compared to the estimated uncertainty in D_{iso}) for both Tensor 1 and Tensor 2 irrespective of the analysis method used. This arises from the fact that the probability densities $P(S^2, \tau_e, R_{ex}, \tau_{m,app}^{(i)}|R_i)$ can have substantial skewness, especially with respect to $\tau_{m,app}^{(i)}$. This is the case for many of the 30 residues in this synthetic data set, except for residues having very small (<10 ps) or large (>200 ps) τ_e values. This skewness results in marginal densities that are biased toward smaller values of $\tau_{m,app}^{(i)}$, even though the maximum of $P(S^2, \tau_e, R_{ex}, \tau_{m,app}^{(i)}|R_i)$ occurs at the correct value of $\tau_{m,app}^{(i)}$. Thus, proteins which have a large number of residues with τ_e values on the order of tens of picoseconds (such as the simulated 30-residue protein used

TABLE 3
Results of Tensor Parameter Estimates for Synthetic Data

	Tensor 1			Tensor 2			Tensor 3		
	SBF	BLW (axial)	BLW (asym)	SBF	BLW (axial)	BLW (asym)	SBF	BLW (axial)	BLW (asym)
D_{iso} (μs^{-1})	14.5 ± 0.1^a (14.0) ^b	14.5 ± 0.1	14.5 ± 0.2	18.5 ± 0.2 (17.7)	18.0 ± 0.2	Mode 1: 18.1 ± 0.2 Mode 2: 18.4 ± 0.3	17.2 ± 0.3 (16.3)	16.4 ± 0.2	Mode 1: 16.4 ± 0.2 Mode 2: 16.5 ± 0.2
R_{axial}	0.99 ± 0.08 (1.0)	0.99 ± 0.08	1.0 ± 0.1	1.9 ± 0.2 (1.8)	1.7 ± 0.2	Mode 1: 1.7 ± 0.2 Mode 2: 0.63 ± 0.07	2.3 ± 0.2 (2.1)	2.1 ± 0.2	Mode 1: 2.0 ± 0.2 Mode 2: 0.45 ± 0.05
R_{asym}	n/a (1.0)	n/a	$>0.93^c$	n/a (1.0)	n/a	Mode 1: >0.80 Mode 2: 0.77 ± 0.06	n/a (0.7)	n/a	Mode 1: 0.70 ± 0.07 Mode 2: 0.65 ± 0.05
ϕ (degrees)	Uniform	Uniform	Uniform	9 ± 7 (10.0)	10 ± 8	Mode 1: 9 ± 8 Mode 2: 5 ± 14	9 ± 5 (10.0)	9 ± 4	Mode 1: 10 ± 5 Mode 2: 10 ± 6
θ (degrees)	Uniform	Uniform	Uniform	31 ± 4 (30.0)	31 ± 4	Mode 1: 31 ± 5 Mode 2: 30 ± 8	35 ± 3 (30.0)	36 ± 3	Mode 1: 32 ± 3 Mode 2: 30 ± 4
χ (degrees)	n/a	n/a	uniform	n/a	n/a	Uniform	n/a (50.0)	n/a	Mode 1: 51 ± 10 Mode 2: 50 ± 9

^a Parameter estimates and errors correspond to the means and standard deviations of the corresponding marginal posterior probability densities.

^b Values in parentheses indicate the values used to generate the synthetic data (reproduced from Table 2 for ease of reference).

^c Lower bounds on R_{asym} correspond to the value of the 5th percentile of the marginal posterior of R_{asym} ; i.e., there is less than a 5% chance (integrated over all the other parameters) that R_{asym} is smaller than the indicated value.

here) can give biased estimates of D_{iso} , while proteins with relatively few residues with τ_e 's in that range will have more accurate estimates of D_{iso} . Such bias would also be propagated into the local dynamical parameters, especially R_{ex} . While the estimate of D_{iso} does differ by more than 5 standard deviations for Tensor 1, the relative error is only 4%, and will result in a systematic overestimation of R_{ex} of at most 0.3 s^{-1} at 400 MHz (based on the linear correlation between R_{ex} and $\tau_{\text{m,app}}^{(i)}$ shown in Fig. 1). It should be noted that the correct value of D_{iso} is also recovered as the uncertainties σ_{ij} approach zero for τ_e values in any regime.

2. Assessment of Statistical Significance

Estimates of the marginal densities $P(R_{\text{axial}}|R)$ and $P(R_{\text{asym}}|R)$ (Figs. 3 and 4) are also extremely useful in that they provide a straightforward method for the determination of the statistical significance of R_{axial} and R_{asym} . From a classical statistical perspective, the statistical significance of a model parameter is often determined via the F statistic, which is related to the ratio of likelihoods for the two hypotheses at the best fit values of the parameters (25). In the Bayesian perspective, the evidence in favor of any given model is given by the

“marginal likelihood of the data,” which is simply the normalization factor $P(R)$ in Eq. [5] or [10]. We can compare the evidence for two competing models by taking the ratio of the marginal likelihoods of the data for each model. This ratio is known as the Bayes factor $B_{1,2}$, and gives the odds in favor of model 1 in the numerator over model 2 in the denominator (assuming that the models are equally likely *a priori*) (18, 26). Furthermore, it follows from its definition that the Bayes factor is symmetric with respect to the hypotheses; i.e., the odds in favor of model 2 ($B_{2,1}$) is simply the reciprocal of the odds in favor of model 1.

In the context of diffusion tensor estimation, there are two hypothesis tests of interest: (1) how much evidence is there for isotropic tumbling and against axially symmetric anisotropic tumbling? and (2) how much evidence is there for fully anisotropic tumbling and against axially symmetric tumbling? These two questions can be answered using the Bayes factors $B_{\text{iso,axial}} = P_{\text{iso}}(R)/P_{\text{axial}}(R)$ and $B_{\text{asym,axial}} = P_{\text{asym}}(R)/P_{\text{axial}}(R)$, where the marginal likelihoods of the data are defined in Eq. [10]. In general, computing a Bayes factor is far from trivial, as it requires knowledge of the normalization constants which ordinarily can be obtained only from multidimensional integrals

which are analytically intractable and difficult to evaluate numerically (26). However, for the case of nested one-dimensional hypotheses (such as those corresponding to $B_{\text{iso,axial}}$ and $B_{\text{asym,axial}}$ above), the Bayes factor can be determined from the marginal prior and posterior densities of the corresponding parameter. In particular (27), if the prior probabilities satisfy the conditions

$$P_{\text{axial}}(D_{\text{iso}}|R_{\text{axial}} = 1) = P_{\text{iso}}(D_{\text{iso}}) \quad [13a]$$

and

$$P_{\text{asym}}(D_{\text{iso}}, R_{\text{axial}}|R_{\text{asym}} = 1) = P_{\text{axial}}(D_{\text{iso}}, R_{\text{axial}}), \quad [13b]$$

then the Bayes factors for isotropic vs axially symmetric and axially symmetric vs fully anisotropic tumbling are given by

$$B_{\text{iso,axial}} = \frac{P_{\text{axial}}(R_{\text{axial}} = 1|R)}{P_{\text{axial}}(R_{\text{axial}} = 1)}, \quad [14a]$$

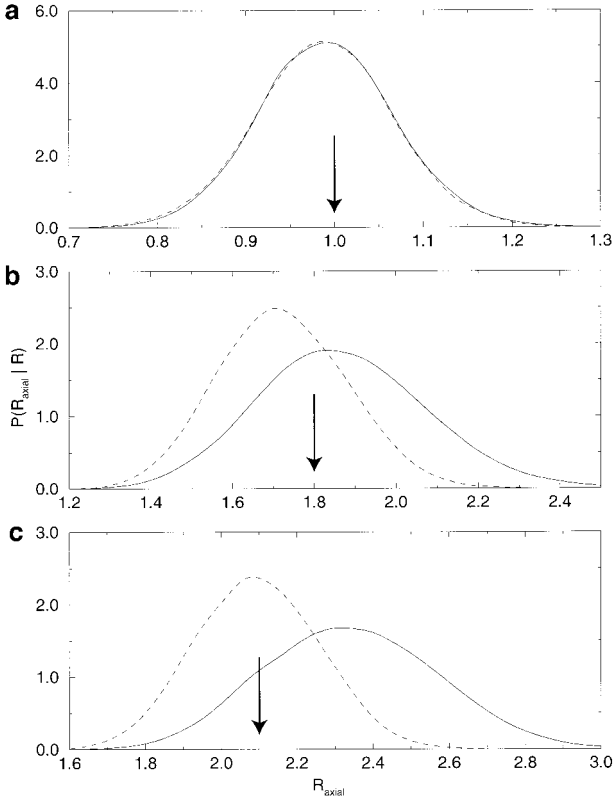


FIG. 3. Plots of the marginal posterior probability densities $P_{\text{axial}}(R_{\text{axial}}|R)$ for Tensor 1 (a), Tensor 2 (b), and Tensor 3 (c), where R_{axial} represents the degree of deviation from isotropic tumbling. The solid and dashed lines represent the estimates of that density using the SBF and BLW(axial) approximations. The arrows represent the values of R_{axial} used to generate the synthetic data.

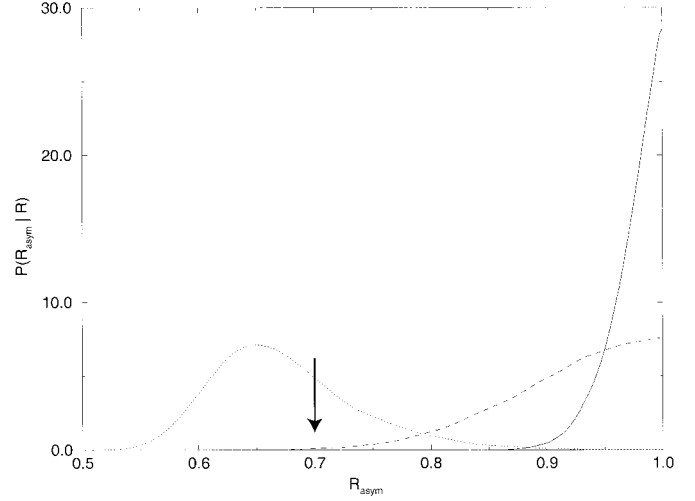


FIG. 4. Plots of the marginal posterior probability densities $P_{\text{asym}}(R_{\text{asym}}|R)$ for Tensor 1 (solid line), Tensor 2 (dashed line), and Tensor 3 (dotted line) using the BLW(asym) approximation. The parameter R_{asym} represents the degree of deviation from axially symmetric tumbling, and the arrow represents the value of R_{asym} used to generate the synthetic data for Tensor 3.

and

$$B_{\text{axial,asym}} = \frac{P_{\text{asym}}(R_{\text{asym}} = 1|R)}{P_{\text{asym}}(R_{\text{asym}} = 1)}, \quad [14b]$$

respectively, where $P_{\text{axial}}(R_{\text{axial}} = 1|R)$ and $P_{\text{asym}}(R_{\text{asym}} = 1|R)$ are the marginal posteriors of Figs. 3 and 4, and $P_{\text{axial}}(R_{\text{axial}} = 1)$ and $P_{\text{asym}}(R_{\text{asym}} = 1)$ are the marginal priors evaluated at $R_{\text{axial}} = 1$ and $R_{\text{asym}} = 1$.³ The conditions of Eq. [13] are satisfied by the priors used here, since Eq. [13a] follows immediately from Eq. [11a], and Eq. [13b] follows from the fact that any value of R_{axial} is consistent with $D_{xx} \leq D_{yy} \leq D_{zz}$ and the conditions of Eqs. [8] and [9] when $R_{\text{asym}} = 1$, i.e., $P_{\text{asym}}(D_{\text{iso}}, R_{\text{axial}}, R_{\text{asym}} = 1) \propto P_{\text{axial}}(D_{\text{iso}}, R_{\text{axial}})$ (see Appendix A).

We can now make use of Eq. [14a] to evaluate the evidence for or against isotropic tumbling based on the marginal posteriors of Fig. 3 and the marginal prior $P_{\text{axial}}(R_{\text{axial}}) = P_0(R_{\text{axial}})$. From Eqs. [A1] and [A2] it follows that given a physically reasonable prior range $\frac{1}{4} \leq R_{\text{axial}} \leq 4$, $P_{\text{axial}}(R_{\text{axial}} = 1) = \frac{1}{6}$, and $B_{\text{iso,axial}} = 6P_{\text{axial}}(R_{\text{axial}} = 1|R)$. For Tensor 1 (Fig. 3a), $P_{\text{axial}}(R_{\text{axial}} = 1|R) \approx 5$ for both the SBF and BLW approximations, which give $B_{\text{iso,axial}} \approx 30$. This means that the odds in favor of isotropic tumbling are 30:1, and constitutes strong evidence against the presence of any anisotropy. For Tensors 2 and 3, $P_{\text{axial}}(R_{\text{axial}} = 1|R)$ is vanishingly small, providing very decisive evidence against isotropic and for axially symmetric or fully anisotropic tumbling. It should be noted that even if there is not decisive evidence in favor of a given model, one

³ In order to simplify the theoretical presentation, we perform the hypothesis testing based on the marginal posteriors and priors obtained after integrating over the angular parameters θ , ϕ , and χ .

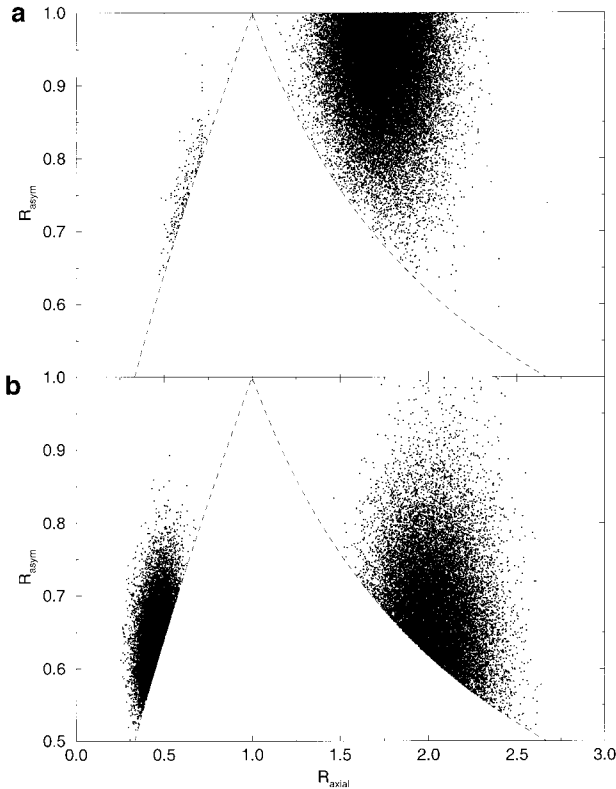


FIG. 5. Monte Carlo samples generated from the posterior probability density $P_{\text{asym}}(D_{\text{iso}}, R_{\text{axial}}, R_{\text{asym}}, \phi, \theta, \chi|R)$ for Tensor 2 (a) and Tensor 3 (b) projected onto the $(R_{\text{axial}}, R_{\text{asym}})$ plane. The dashed lines indicate the regions of the $(R_{\text{axial}}, R_{\text{asym}})$ plane consistent with the definitions of those parameters, and correspond to the curves for which $D_{zz}/D_{yy} = D_{yy}/D_{xx}$ and the distinction between “prolate-like” and “oblate-like” is ill defined. The right-hand region corresponds to “prolate-like” ($D_{zz}/D_{yy} > D_{yy}/D_{xx}$), while the left-hand region corresponds to “oblate-like” ($D_{zz}/D_{yy} < D_{yy}/D_{xx}$) ellipsoids.

can simply perform the analysis using the larger of the nested models. The resulting parameter estimates will then represent an “average” (in some sense) over the models which are supported by the data.

We can similarly determine the evidence for or against axially symmetric vs fully anisotropic tumbling from Eq. [14b]. In this case, we must obtain the marginal prior $P_{\text{asym}}(R_{\text{asym}})$, which is derived in Appendix A. Substituting the prior range over R_{axial} into Eq. [A3], we find that $P_{\text{asym}}(R_{\text{asym}} = 1) \approx 2.4$. From the marginal posterior densities of Fig. 4 we see that $P_{\text{asym}}(R_{\text{asym}} = 1|R) \approx 28.5, 7.6,$ and 0.02 for Tensors 1, 2 and 3, respectively. This gives Bayes factors $B_{\text{axial,asym}} \approx 12, 3,$ and 0.008 , respectively. Although there is a greater than 1:1 odds in favor of axially symmetric tumbling for Tensors 1 and 2, according to the conventions of the Bayesian statistics literature (26) Bayes factors of this magnitude do not constitute very strong evidence. On the other hand, there is very strong evidence in favor of fully anisotropic tumbling for Tensor 3 (with $B_{\text{asym,axial}} = B_{\text{axial,asym}}^{-1} \approx 125$).

3. Comparison with a “Standard” Approach for Estimation of Tensor Parameters

A. Synthetic data. It is informative to compare the results obtained above to those obtained using the approach often used in the current literature, namely the elimination of residues with significant τ_e and/or R_{ex} values, followed by the estimation of apparent τ_m values from R_2/R_1 and fitting of those to a diffusion tensor (16, 17). In order to estimate overall tumbling parameters from R_2/R_1 , it is first necessary to identify and eliminate residues which have significant contributions from $\tau_e \neq 0$ and/or $R_{\text{ex}} \neq 0$. Residues with τ_e values in the neighborhood of $\tau_e = 0.1 \tau_m$ have NOE values which are significantly reduced from those with $\tau_e = 0$. Therefore, such residues can be identified and eliminated by discarding all residues with NOE values below some cutoff (e.g., $\text{NOE} < 0.65$). It should be noted that due to the dependence of the NOE on τ_e , this criterion will not detect residues with τ_e values greater than $\approx 0.25 \tau_m$, even though such residues will still have significantly perturbed R_2/R_1 values (4). After removal of residues with nonzero τ_e contributions, one can use Eq. [1] to remove residues with nonzero R_{ex} contributions. This criterion was motivated by the observation that in the presence of rotational anisotropy, bond vectors aligned along the long axis of the diffusion tensor will experience an increase in R_2 which is correlated with a decrease in R_1 (7), while R_{ex} only has an effect on R_2 . Therefore, eliminating residues which have larger than average R_2 values and not smaller than average R_1 values will tend to eliminate residues with significant R_{ex} contributions.

As is well known, in the limit of $\tau_e = 0$ and $R_{\text{ex}} = 0$, the ratio R_2/R_1 is independent of S^2 , and can be used to estimate the apparent overall tumbling correlation time $\tau_{\text{m,app}}^{(i)}$ or apparent rotational diffusion coefficient $D_{\text{app}}^{(i)} = (6\tau_{\text{m,app}}^{(i)})^{-1}$ for each residue i . These apparent diffusion coefficients can then be related to the diffusion tensor parameters and bond vector orientations via the BLW approximation,

$$(x_i y_i z_i) \begin{pmatrix} Q_{11} & Q_{12} & Q_{13} \\ Q_{12} & Q_{22} & Q_{23} \\ Q_{13} & Q_{23} & Q_{33} \end{pmatrix} \begin{pmatrix} x_i \\ y_i \\ z_i \end{pmatrix} = D_{\text{app}}^{(i)}, \quad [15]$$

where (x_i, y_i, z_i) are the direction cosines of the i th bond vector in the molecular frame and Q_{ij} are the same as in Eq. [4] except that they are in the *molecular* frame and not the PAS of the tensor (16). Equation [15] is linear in the unknowns Q_{ij} , and the set of linear equations corresponding to Eq. [15] for all i ($i = 1, \dots, N$) can be rewritten in matrix form as

$$\begin{pmatrix} x_1^2 & 2x_1y_1 & y_1^2 & 2x_1z_1 & 2y_1z_1 & z_1^2 \\ x_2^2 & 2x_2y_2 & y_2^2 & 2x_2z_2 & 2y_2z_2 & z_2^2 \\ \vdots & \vdots & \vdots & \vdots & \vdots & \vdots \\ x_N^2 & 2x_Ny_N & y_N^2 & 2x_Nz_N & 2y_Nz_N & z_N^2 \end{pmatrix} \begin{pmatrix} Q_{11} \\ Q_{12} \\ Q_{22} \\ Q_{13} \\ Q_{23} \\ Q_{33} \end{pmatrix} = \begin{pmatrix} D_{\text{app}}^{(1)} \\ D_{\text{app}}^{(2)} \\ \vdots \\ D_{\text{app}}^{(N)} \end{pmatrix}, \quad [16]$$

which can be solved by standard linear algebraic methods. In particular, if we assume that the uncertainty in $D_{\text{app}}^{(i)}$ is normally distributed with standard deviation σ_i (as described below), then the maximum likelihood solution for the Q_{ij} 's is given by weighted least-squares fit

$$\begin{pmatrix} Q_{11} \\ Q_{12} \\ Q_{22} \\ Q_{13} \\ Q_{23} \\ Q_{33} \end{pmatrix} = [A^T \text{diag}(\sigma_1^{-2} \sigma_2^{-2} \cdots \sigma_N^{-2}) A]^{-1} \times A^T \text{diag}(\sigma_1^{-2} \sigma_2^{-2} \cdots \sigma_N^{-2}) \begin{pmatrix} D_{\text{app}}^{(1)} \\ D_{\text{app}}^{(2)} \\ \vdots \\ D_{\text{app}}^{(N)} \end{pmatrix}, \quad [17]$$

where A is the matrix of direction cosines on the left-hand side of Eq. [16], and $\text{diag}(\cdots)$ is a diagonal matrix having the indicated elements along the diagonal.

We performed the calculation described above using the data for Tensor 1 (corresponding to isotropic tumbling). Application of the $\text{NOE} > 0.65$ criterion resulted in the elimination of residues 3, 4, 7–10, 12, 13, 15, 22, 24–26, 28, and 29. The criterion of Eq. [1] further eliminated residues 11 and 18. The uncertainty in R_2/R_1 for the remaining 13 residues was assumed to be normal, with a variance estimated by propagation of errors (28) using the same 5% relative errors used in the Bayesian analysis above. The value and uncertainty in each $D_{\text{app}}^{(i)}$ were estimated using a classical Monte Carlo approach by calculating $D_{\text{app}}^{(i)}$ by numerical root finding using *Mathematica* (29) for 2000 pseudorandom numbers drawn from the corresponding normal R_2/R_1 distribution, and using the variance of the resulting $D_{\text{app}}^{(i)}$ values as the variance of the assumed normal uncertainty in $D_{\text{app}}^{(i)}$. The best fit diffusion tensor elements were then determined using Eq. [17].

After diagonalization of the best fit Q matrix, the solution for fitting the data generated using an isotropic system with a fully anisotropic tumbling model was found to be $D_{xx} = 11.5 \mu\text{s}^{-1}$, $D_{yy} = 12.5 \mu\text{s}^{-1}$, and $D_{zz} = 16.5 \mu\text{s}^{-1}$, corresponding to reparametrized values of $D_{\text{iso}} = 13.5 \mu\text{s}^{-1}$, $R_{\text{axial}} = 1.38$, and $R_{\text{asym}} = 0.92$. To assess the statistical significance of this fit over isotropic tumbling, the fit was repeated with the constraints $Q_{ij} = 0$ for $i \neq j$ and $Q_{11} = Q_{22} = Q_{33}$. The isotropic fit also gave $D_{\text{iso}} = 13.5 \mu\text{s}^{-1}$, and the F statistic for the improvement in the fit using the anisotropic model (17) was found to be 5.74, corresponding to a very significant p value of 0.002. Therefore, straightforward application of methods currently used in the literature for estimation of rotational diffusion anisotropy to small data sets can potentially produce misleading results, such as the one described here, in which synthetic data generated using an isotropic tumbling model result in a statistically significant estimated anisotropy of $\approx 1.4:1$. The origin of this erroneous result is that application of

Eq. [1] failed to eliminate four residues with nonzero R_{ex} contributions (residues 6, 16, 19, and 21), and the resulting deviations in the R_2/R_1 values for those residues were propagated into a fictional anisotropy. Although a visual inspection of the $D_{\text{app}}^{(i)}$ values as a function of orientation would reveal that residues 6, 16, 19, and 21 are probably outliers above an otherwise flat “baseline,” this cannot be detected by F testing alone. A more sophisticated criterion that takes advantage of the quadratic field dependence of R_{ex} such as that proposed by Phan *et al.* (14) could be used instead of Eq. [1] to detect and eliminate residues with R_{ex} contributions. The marginal posterior densities of $\tau_{\text{m,app}}^{(i)}$ do not suffer from this problem, however, and estimation of the tensor parameters finds very strong evidence (odds of $>300:1$) in favor of isotropic vs fully anisotropic tumbling without the need to exclude any data.

We repeated this calculation for the fully anisotropic Tensor 3 data, and found that the NOE and Eq. [1] criteria eliminated the same 17 residues as for Tensor 1. In this case, the best fit fully anisotropic tensor was found to be $D_{xx} = 9.0 \mu\text{s}^{-1}$, $D_{yy} = 14.1 \mu\text{s}^{-1}$, and $D_{zz} = 23.1 \mu\text{s}^{-1}$, corresponding to reparametrized values of $D_{\text{iso}} = 15.4 \mu\text{s}^{-1}$, $R_{\text{axial}} = 2.0$, and $R_{\text{asym}} = 0.64$. The isotropic fit gave $D_{\text{iso}} = 15.6 \mu\text{s}^{-1}$, and the F statistic for the improvement in the fit was found to be 34.7, corresponding to a vanishingly small p value. In contrast to the results for Tensor 1, the results are much closer to the correct values (Table 2). This striking difference is due to the fact that the variation in $D_{\text{app}}^{(i)}$ as a function of orientation due to anisotropy for Tensor 3 is comparable in magnitude to the perturbations in $D_{\text{app}}^{(i)}$ due to the small R_{ex} contributions in residues 6, 16, 19, and 21, and therefore they contribute much less to the overall fit.

B. Experimental data. To demonstrate the applicability of this method to real experimental data and to compare its performance to the “standard” method, we performed a tensor estimation calculation for relaxation data obtained on the dimeric Ca^{2+} binding protein S100B($\beta\beta$) (91 residues/monomer). S100B($\beta\beta$) is an EF-hand type Ca^{2+} binding protein that has been implicated in the neuropathologies of Down’s syndrome and Alzheimer’s disease (30), and its structure has been determined by NMR methods (31, 32). Estimates of the marginal $\tau_{\text{m,app}}^{(i)}$ densities for the 65 residues for which R_1 , R_2 , and NOE data were available at both 400 and 600 MHz were generated using Eqs. [5]–[7] as described above. An estimate of the diffusion tensor parameters for both axially symmetric and fully anisotropic tumbling was then made from the marginal $\tau_{\text{m,app}}^{(i)}$ densities using the BLW approximation. Information regarding the dimeric nature of S100B($\beta\beta$) was included in the calculation by using orientations for 130 bond vectors, corresponding to the 65 residues in each of the two monomer units. Identical $P(\tau_{\text{m,app}}^{(i)}|R_i)$ densities were assigned to each of the symmetry-related residues. The molecular frame was chosen to coincide with the inertia tensor of the protein structure as determined by NMR methods, with the dimer C_2 symmetry axis along the x axis of the molecular frame ($\theta = 90^\circ$, $\phi = 0^\circ$).

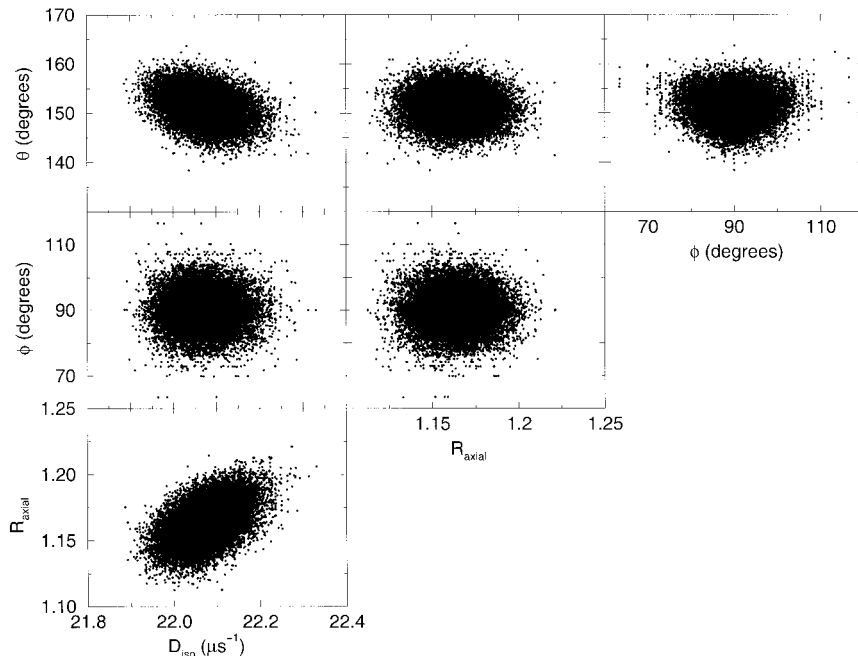


FIG. 6. Monte Carlo samples generated from the posterior probability density $P_{\text{axial}}(D_{\text{iso}}, R_{\text{axial}}, \phi, \theta|R)$ using the BLW(axial) approximation based on experimental relaxation data obtained on the protein S100B($\beta\beta$) (the χ dimension has been dropped since $R_{\text{axial}} > 1$ for all points and χ represents rotations about the symmetry axis). Each panel corresponds to a projection of the full set of Monte Carlo samples onto a plane corresponding to each pair of parameters.

As a test, the calculation was repeated without the symmetry information, and the results were consistent with those presented below, albeit with much larger uncertainties for the tensor parameters. Less than 2 h of CPU time on an SGI R10000 processor was required for these calculations.

A summary of the resulting tensor fit is shown in Figs. 6 and 7. The lack of Monte Carlo samples at $R_{\text{axial}} = 1$ in Fig. 6 indicates that the marginal posterior density $P(R_{\text{axial}} = 1|R)$ is

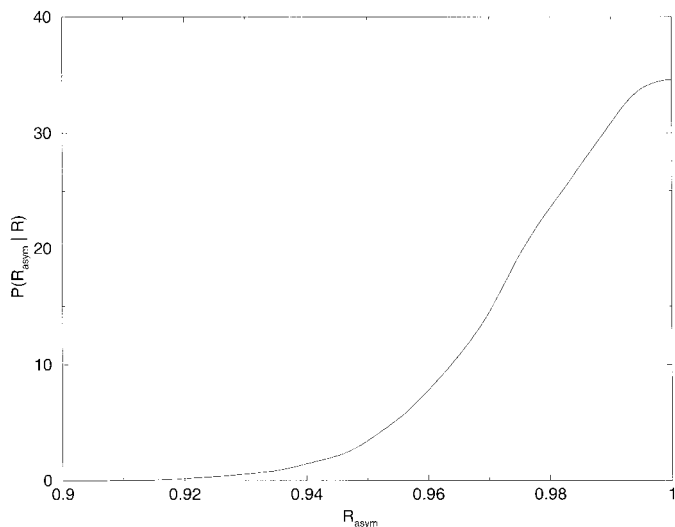


FIG. 7. Plot of the marginal posterior probability density $P_{\text{asym}}(R_{\text{asym}}|R)$ generated using the BLW(asym) approximation based on experimental relaxation data obtained on the protein S100B($\beta\beta$).

vanishingly small, which implies overwhelming evidence against isotropic tumbling. The expectation values and standard deviations for the axially symmetric tensor parameter estimation Monte Carlo are $D_{\text{iso}} = 22.3 \pm 0.1 \mu\text{s}^{-1}$, $R_{\text{axial}} = 1.17 \pm 0.02$, $\theta = 151^\circ \pm 5^\circ$, and $\phi = 90^\circ \pm 8^\circ$. It is expected that for a symmetric dimer the symmetry axis of the diffusion tensor should be either coincident with or perpendicular to the C_2 axis for the dimer. It is clear, based on this analysis, that the latter is the case for S100B($\beta\beta$). Based on the marginal posterior density $P(R_{\text{asym}}|R)$ from the fully anisotropic fit (Fig. 7), we find that $P(R_{\text{asym}} = 1|R) \approx 22$, implying an odds of 9:1 against fully anisotropic tumbling and for axially symmetric tumbling (based on the priors used under Section 2 of Results, above).

For comparison, the data were also subjected to a “standard” analysis of global diffusion. First, those residues for which $\text{NOE} < 0.65$ at 600 MHz (two C-terminal residues) or was not known (8 weak or absent and 8 due to overlap at 600 MHz) were eliminated from consideration, due to possible τ_c contributions. After application of the criterion of Eq. [1], 7 of those remaining residues were eliminated due to possible exchange contributions to T_2 relaxation. Local effective correlation times of the remaining 66 residues were calculated on the basis of the 600-MHz T_1/T_2 ratios using the program R2R1_TM (A. G. Palmer, Columbia University). Using these correlation times, initial estimates of global diffusion parameters were estimated by the approach of Brüschweiler *et al.* (16) and Lee *et al.* (17), using the program QUADRIC_DIFFUSION, version 1.1 (A. G. Palmer, Columbia University). Isotropic, axially sym-

metric, and fully anisotropic ellipsoidal diffusion tensor parameters were estimated and then subjected to statistical F testing. Two axial diffusion tensors were found to fit the data with statistically significant improvement over the isotropic fit. One was oblate ($D_{\text{iso}} = 21.3 \pm 0.1 \mu\text{s}^{-1}$, $R_{\text{axial}} = 0.89 \pm 0.01$; $p < 10^{-3}$) compared to isotropic, and the other prolate ($D_{\text{iso}} = 21.5 \pm 0.1 \mu\text{s}^{-1}$, $R_{\text{axial}} = 1.16 \pm 0.01$; $p < 10^{-10}$). Although no classical statistical test is available to test the two tensors against each other, the prolate tensor displayed a χ^2_ν lower than that of the oblate. Each was subjected to an F test, comparing an axial tensor to the best fit fully anisotropic tensor ($D_{\text{iso}} = 21.5 \pm 0.1 \mu\text{s}^{-1}$, $R_{\text{axial}} = 1.16 \pm 0.01$, $R_{\text{asym}} = 0.98 \pm 0.01$). The anisotropic tensor did not show improvement when compared to the prolate tensor ($p \approx 0.8$), whereas significant improvement was shown when compared to the oblate tensor ($p < 10^{-6}$). At 400 MHz, 7 additional residues were lost to weak signal or overlap, and the analysis was repeated for the remaining 59 residues. Again, both oblate and prolate tensors were found to fit the data better than the best isotropic model with a high degree of statistical significance ($p < 10^{-6}$ and $p < 10^{-18}$, respectively). The oblate result ($D_{\text{iso}} = 21.1 \pm 0.1 \mu\text{s}^{-1}$, $R_{\text{axial}} = 0.89 \pm 0.01$) allowed significant improvement in moving to a fully anisotropic tensor ($D_{\text{iso}} = 21.3 \pm 0.1 \mu\text{s}^{-1}$, $R_{\text{axial}} = 1.16 \pm 0.01$, $R_{\text{asym}} = 0.98 \pm 0.01$, $p < 10^{-12}$), whereas the prolate result ($D_{\text{iso}} = 21.3 \pm 0.1 \mu\text{s}^{-1}$, $R_{\text{axial}} = 1.16 \pm 0.01$) did not ($p \approx 0.7$). Since for both the 400- and 600-MHz data the prolate axially symmetric tensor was nearly identical to the best fit fully anisotropic tensor (with $R_{\text{axial}} = 1.16$ and $R_{\text{asym}} \approx 1$), and the best fit fully anisotropic tensor in each case represented a significant improvement over the oblate axially symmetric tensor, only the prolate axially symmetric tensor was considered further.

An initial estimate of the diffusion tensor parameters based on the above analysis was used as a starting point for a complete Lipari–Szabo analysis of internal motional parameters. Data collected at both fields were used simultaneously, and the motional parameters S^2 , τ_e , and R_{ex} were optimized. An iterative process was performed in which model selection by statistical F testing was alternated with optimization of global diffusion parameters, following in large part the method of Mandel *et al.* (33), and using the software MODELFREE version 4.0.1 (A. G. Palmer, Columbia University). For diffusion optimization, only those residues were considered whose data were found to fit well to model 1 (only S^2 is optimized), 2 (S^2 , τ_e), 3 (S^2 , R_{ex}), or 4 (S^2 , τ_e , R_{ex}). Goodness of fit was judged by a χ^2 test at the $p = 0.1$ significance level, and an F test at $p = 0.2$ significance was used to discern genuine improvements in the fit for more complex models. For each residue, the simplest model to pass these criteria was used. Several rounds of calculations alternating model selection and diffusion tensor optimization converged (with little variation) on a diffusion tensor with parameters $D_{\text{iso}} = 21.4 \pm 0.1 \mu\text{s}^{-1}$, $R_{\text{axial}} = 1.16 \pm 0.03$, $\theta = 141 \pm 4^\circ$, and $\phi = 90^\circ$. For computational efficiency, the coordinates of only one subunit were included in the MODELFREE runs, while ϕ was con-

strained to 90° to maintain the condition of C_2 symmetry about the x axis.⁴ A total of approximately 60 h of CPU time on an SGI R10000 processor was required for these calculations. Details of the complete analysis, as well as a comparison of the results for internal motion using MODELFREE to those using the Bayesian marginal density approach, will be published elsewhere. The tensor parameter estimates are obviously in very good agreement. Only the estimates of D_{iso} differ significantly compared to the estimated uncertainties, with the Bayesian estimate being larger by $\approx 1 \mu\text{s}^{-1}$, and are consistent with possible bias due to skewness of the posterior probability density, as described above.

DISCUSSION

We have shown that the use of marginal probability densities for $\tau_{\text{m,app}}^{(i)}$ based only on R_1 , R_2 , and NOE data collected at two easily accessible spectrometer field strengths (400 and 600 MHz) can be used to reliably detect, quantify, and assess the statistical significance of rotational diffusion anisotropy in macromolecules without making assumptions about the nature and distributions of internal motions. In particular, the field strength dependence of the chemical exchange contribution to R_2 can be used to separate the effects of chemical exchange and anisotropy without the need for additional experimental data from rotating frame or cross-correlated relaxation experiments. However, it should be noted that the formalism presented here can easily accommodate such data with no change whatsoever to the overall theory, since such data could be incorporated at the level of the likelihood and prior densities in Eq. [5]. For example, independent knowledge of R_{ex} obtained from rotating frame relaxation dispersion experiments could be used to reduce the width of the marginal densities of $\tau_{\text{m,app}}^{(i)}$ due to the correlation among those two parameters (Fig. 2).

In general, both the SBF and BLW approximations perform well, with the BLW providing slightly more accurate estimates of D_{iso} as well as allowing for the estimation of fully anisotropic tumbling tensor parameters. Although the authors indicate that the BLW approximation is valid only for small anisotropies (16), our results indicate that it can still give excellent estimates of the diffusion tensor parameters even for anisotropies on the order of 2:1 (Table 3). Therefore, unless the expected anisotropy is quite large (substantially greater than 2:1), the BLW approximation seems to be the method of choice for tensor parameter estimation.

Given the very different data analysis strategies of the Bayesian and “standard” approaches, it is interesting and reassuring that the resulting tensor parameter estimates generally agree very well (except for the case of the Tensor 1 synthetic data). The amount of CPU time required for the two calcula-

⁴ A comparison was made of two runs of MODELFREE in which the only difference was that one used coordinates from a single subunit while holding ϕ at 90° , and the other used both subunits and allowed ϕ to float. Though the latter took considerably more CPU time, the tensor parameter estimates were indistinguishable.

tions, however, is significantly different, especially when using MODELFREE to estimate uncertainties in the diffusion tensor parameters. Although reasonable search parameters were chosen for the MODELFREE analysis of the experimental data, it is possible that the calculations could have been performed in less time. The Bayesian approach avoids the guesswork involved in choosing the parameter space sampling, and in this case required less total CPU time by approximately a factor of 30. This is due to the fact that the marginal $P(\tau_{m,app}^{(i)}|R_i)$ densities summarize the tumbling correlation time information more efficiently, and due to the avoidance of computationally intensive nonlinear optimization (4). It should be noted, however, that this comparison is appropriate only if the desired end product is the tensor parameter estimate. This is because the MODELFREE calculation also provides final estimates of the internal motional parameters, whereas in the Bayesian approach, the global tensor parameter information would still have to be propagated back into the local parameter estimates (4). We estimate that even in that case, the Bayesian approach is at least a factor of 6 faster.

The ability of the Bayesian approach to disentangle the effects of chemical exchange and anisotropy with a minimal amount of experimental data suggests that if more data, particularly from transverse and longitudinal cross-correlated relaxation (12), were collected and analyzed in this manner, one might be able to address questions about other contributions to ^{15}N relaxation. One such question which has attracted some interest recently involves the possible variations in the magnitude and orientation of the ^{15}N CSA tensor (21–23). Such variations are of particular interest since they can affect the performance of NMR experiments based on the TROSY method (34, 35).

CONCLUSIONS

In conclusion, our formalism not only provides accurate estimates of the “best fit” tensor parameter values, but the posterior probability density function provides a full characterization of the uncertainty in the tensor parameters, including any statistical correlations, skewness, and multimodality. Furthermore, it provides a simple way to assess the statistical significance of different models for the diffusion tensor in terms of Bayes factors, all with very reasonable amounts of computer time. We have validated the accuracy and utility of our methodology with synthetic data, and have demonstrated an application to real experimental data. Although our approach requires more than the three standard relaxation measurements per residue, access to multiple spectrometers is becoming more common, and the collection of relaxation data at multiple field strengths is becoming more routine. We believe that the use of multiple field strengths and relaxation types (such as cross-correlated relaxation) will be critical for reliably disentangling the effects of anisotropy, chemical exchange, and variations in chemical shift anisotropy. The statistical approach described in this paper provides a simple,

reliable, and efficient tool for the simultaneous analysis of these data. Software implementing this approach will be available at <http://www-nmr.cabm.rutgers.edu>.

APPENDIX A

A normalizable (“proper”) prior $P_{\text{axial}}(R_{\text{axial}})$ can be constructed in several ways. The simplest is to define a range $(R_{\text{axial}}^{(\min)}, R_{\text{axial}}^{(\max)})$ over which $P_{\text{axial}}(R_{\text{axial}})$ is equal to a nonzero constant, and set $P_{\text{axial}}(R_{\text{axial}}) = 0$ outside of that range. However, such a prior suffers from an asymmetry in its treatment of prolate- and oblate-like ellipsoids. Suppose that one wished to represent the highly uninformative prior knowledge that the tensor is prolate with an undefined upper bound (i.e., $1 \leq D_{\parallel}/D_{\perp} < \infty$). Such a prior over R_{axial} would obviously be improper, since it is equal to a constant over an unbounded region. On the other hand, the analogous prior for oblate tensors would be equal to a constant over the *bounded* region $0 < R_{\text{axial}} \leq 1$, leading to a proper prior over R_{axial} . In order to treat prolate and oblate tensors on more equal terms, we define the prior $P_{\text{axial}}(R_{\text{axial}})$ such that D_{\parallel}/D_{\perp} is uniformly distributed for prolate tensors, while D_{\perp}/D_{\parallel} is uniformly distributed for oblate tensors (for $R_{\text{axial}} = 1$). After accounting for the change of variable $R_{\text{axial}} = (D_{\perp}/D_{\parallel})^{-1}$ (36), this leads to

$$P_{\text{axial}}(R_{\text{axial}}) = \begin{cases} 0, & R_{\text{axial}} < R_{\text{axial}}^{(\min)} \leq 1 \\ kR_{\text{axial}}^{-2}, & R_{\text{axial}}^{(\min)} \leq R_{\text{axial}} \leq 1 \\ k, & 1 > R_{\text{axial}} \geq R_{\text{axial}}^{(\max)} \\ 0, & R_{\text{axial}} > R_{\text{axial}}^{(\max)} \end{cases} \quad [\text{A1}]$$

where the normalization constant k is given by

$$k = \frac{R_{\text{axial}}^{(\min)}}{1 + R_{\text{axial}}^{(\min)}(R_{\text{axial}}^{(\max)} - 2)} \quad [\text{A2}]$$

for $0 < R_{\text{axial}}^{(\min)} < 1$ and $R_{\text{axial}}^{(\max)} > 1$. For all calculations in this paper, we will choose $R_{\text{axial}}^{(\min)} = \frac{1}{4}$ and $R_{\text{axial}}^{(\max)} = 4$. It should be noted that the choice of prior range typically has minimal effect on the parameter estimation problem, since the prior is normally much flatter than the likelihood function. On the other hand, the prior can have a more substantial effect on the Bayes factors (Eq. [14]), as discussed under Results.

In the fully anisotropic case, the prior over R_{axial} and R_{asym} cannot be factored into independent R_{axial} and R_{asym} contributions, since not all points in the $(R_{\text{axial}}, R_{\text{asym}})$ plane are feasible *a priori*. It can be shown that the definitions of R_{axial} and R_{asym} imply a joint prior $P_{\text{asym}}(R_{\text{axial}}, R_{\text{asym}}) \propto P_{\text{axial}}(R_{\text{axial}})f(R_{\text{axial}}, R_{\text{asym}})$, where the function $f(R_{\text{axial}}, R_{\text{asym}})$ is equal to 1 in the regions bounded by the curves $R_{\text{asym}} = 1$ and

$$\frac{2R_{\text{asym}}^2}{(1 + R_{\text{asym}})} = R_{\text{axial}}$$

for $R_{\text{axial}} \leq 1$ (i.e., the region where $R_{\text{axial}} \leq 1$, $D_{zz}/D_{yy} < D_{yy}/D_{xx}$, and $D_{xx} \leq D_{yy} \leq D_{zz}$), and $R_{\text{axial}} = 1$ and $R_{\text{axial}}(1 + R_{\text{axial}}) = R_{\text{axial}}$ for $R_{\text{axial}} > 1$ (i.e., the region where $R_{\text{axial}} \geq 1$, $D_{zz}/D_{yy} > D_{yy}/D_{xx}$, and $D_{xx} \leq D_{yy} \leq D_{zz}$), and 0 elsewhere. Although the full normalized expression for $P_{\text{axym}}(R_{\text{axial}}, R_{\text{axym}})$ is quite cumbersome and will not be given here, the normalized marginal prior density $P_{\text{axym}}(R_{\text{axym}})$ evaluated at $R_{\text{axym}} = 1$ (which is required for testing for fully anisotropic tumbling using Eq. [14b]) is given by the very simple expression

$$P_{\text{axym}}(R_{\text{axym}} = 1) = R_{\text{axial}}^{(\text{max})} + (R_{\text{axial}}^{(\text{min})})^{-1} - 2 \quad [\text{A3}]$$

for $0 < R_{\text{axial}}^{(\text{min})} < 1$ and $R_{\text{axial}}^{(\text{max})} > 1$.

APPENDIX B

Monte Carlo sampling from the densities $P(S^2, \tau_e, R_{\text{ex}}, \tau_{\text{m,app}}^{(i)} | R_i)$, $P_{\text{axial}}(D_{\text{iso}}, R_{\text{axial}}, \phi, \theta | R)$, and $P_{\text{axym}}(D_{\text{iso}}, R_{\text{axial}}, R_{\text{axym}}, \phi, \theta, \chi | R)$ was accomplished using the Gibbs algorithm (37), which is a special case of the Metropolis algorithm (38) in which moves are made using points generated from conditional densities, thereby ensuring an acceptance probability of 1. In order to avoid the often strong nonlinear correlations between S^2 and τ_e (39, 40), the sampling from $P(S^2, \tau_e, R_{\text{ex}}, \tau_{\text{m,app}}^{(i)} | R_i)$ was performed in the reparametrized space $(J_{\text{N}}, J_{\text{H}}, R_{\text{ex}}, \tau_{\text{m,app}}^{(i)})$, where J_{N} and J_{H} are the Lipari–Szabo spectral densities calculated using Eq. [2] as a function of S^2 , τ_e , and $\tau_{\text{m,app}}^{(i)}$ at the Larmor frequencies of ^{15}N and ^1H at 400 MHz proton frequency. Sampling from the univariate conditional densities was performed with a “slicing” algorithm using the “stepping-out” method (41) and sampling widths of 0.005, 0.0005, 0.1, and 0.5 for J_{N} , J_{H} , R_{ex} , and $\tau_{\text{m,app}}^{(i)}$, and 10.0, 10.0, 2.0, 30.0, 30.0, and 30.0 for D_{iso} , R_{axial} , R_{axym} , ϕ , θ , and χ , respectively. In order to make sampling from correlated densities more efficient, the “overrelaxation” method described by Neal (41) was used for 40 consecutive iterations, interspersed with one simple Gibbs iteration.

The marginal posterior density $P(\tau_{\text{m,app}}^{(i)} | R_i)$ for each residue i was estimated from the Monte Carlo samples using a univariate Gaussian kernel density estimator (42) from the Monte Carlo samples,

$$P(\tau_{\text{m,app}}^{(i)} | R_i) \approx \frac{1}{\sqrt{2\pi}Kh} \sum_{j=1}^K \exp\left(-\frac{(\tau_{\text{m,app}}^{(i)} - [\tau_{\text{m,app}}^{(i)}]_j)^2}{2h^2}\right), \quad [\text{B1}]$$

where $[\tau_{\text{m,app}}^{(i)}]_j$ is the $\tau_{\text{m,app}}^{(i)}$ component of the j th Monte Carlo sample from $P(S^2, \tau_e, R_{\text{ex}}, \tau_{\text{m,app}}^{(i)} | R_i)$, K is the total number of Monte Carlo samples used to construct the density estimate, and the “window width” h was chosen using Terrell’s “maximal smoothing” criterion (43) based on the standard deviation of the $[\tau_{\text{m,app}}^{(i)}]_j$ points. For improved computational efficiency in the tensor estimation calculations, the logarithm of each mar-

ginal density $P(\tau_{\text{m,app}}^{(i)} | R_i)$ was represented in the form of a Chebycheff polynomial expansion (44) of order 40 in all subsequent calculations.

ACKNOWLEDGMENTS

This research was supported by the National Institutes of Health (NRSA Fellowship GM19856-02 to M.A. and Grants GM-58888 to D.J.W., GM-30580 to R.M.L., and GM-50733 to G.T.M.) and the American Cancer Society (RPG0004001-CCG to D.J.W.). Support for CABM structural biology computing facilities was provided by a grant from the W. M. Keck Foundation.

REFERENCES

1. A. G. Palmer III, Probing molecular motions by NMR, *Curr. Opinion Struct. Biol.* **7**, 732–737 (1997).
2. M. W. F. Fischer, A. Majumdar, and E. R. P. Zuiderweg, Protein NMR relaxation: Theory, applications and outlook, *Prog. NMR Spectrosc.* **33**, 207–272 (1998).
3. J. M. Schurr, H. P. Babcock, and B. S. Fujimoto, A test of the model-free formulas. Effects of anisotropic rotational diffusion and dimerization, *J. Magn. Reson. B* **105**, 211–224 (1994).
4. M. Andrec, G. T. Montelione, and R. M. Levy, Estimation of dynamic parameters from NMR relaxation data using the Lipari–Szabo model-free approach and Bayesian statistical methods, *J. Magn. Reson.* **139**, 408–421 (1999).
5. P. Luginbühl, K. V. Pervushin, H. Iwai, and K. Wüthrich, Anisotropic molecular rotational diffusion in ^{15}N spin relaxation studies of protein mobility, *Biochemistry* **36**, 7305–7312 (1997).
6. E. de Alba, J. L. Barber, and N. Tjandra, The use of residual dipolar coupling in concert with backbone relaxation rates to identify conformational exchange by NMR, *J. Am. Chem. Soc.* **121**, 4282–4283 (1999).
7. G. Barbato, M. Ikura, L. E. Kay, R. W. Pastor, and A. Bax, Backbone dynamics of calmodulin studied by ^{15}N relaxation using inverse detected two-dimensional NMR spectroscopy: The central helix is flexible, *Biochemistry* **31**, 5269–5278 (1992).
8. N. Tjandra, P. Wingfield, S. Stahl, and A. Bax, Anisotropic rotational diffusion of perdeuterated HIV protease from ^{15}N NMR relaxation measurements at two magnetic fields, *J. Biomol. NMR* **8**, 273–284 (1996).
9. T. Szyperski, P. Luginbühl, G. Otting, P. Güntert, and K. Wüthrich, Protein dynamics studied by rotating frame ^{15}N spin relaxation times, *J. Biomol. NMR* **3**, 151–164 (1993).
10. M. Akke, J. Liu, J. Cavanagh, H. P. Erickson, and A. G. Palmer III, Pervasive conformational fluctuations on microsecond time scales in a fibronectin type III domain, *Nature Struct. Biol.* **5**, 55–59 (1998).
11. A. E. Meekhof and S. M. V. Freund, Separating the contributions to ^{15}N transverse relaxation in a fibronectin type III domain, *J. Biomol. NMR* **14**, 13–22 (1999).
12. C. D. Kroenke, J. P. Loria, L. K. Lee, M. Rance, and A. G. Palmer III, Longitudinal and transverse ^1H – ^{15}N dipolar/ ^{15}N chemical shift anisotropy relaxation interference: Unambiguous determination of rotational diffusion tensors and chemical exchange effects in biological macromolecules, *J. Am. Chem. Soc.* **120**, 7905–7915 (1998).
13. N. Tjandra, H. Kuboniwa, H. Ren, and A. Bax, Rotational dynamics of calcium-free calmodulin studied by ^{15}N -NMR relaxation measurements, *Eur. J. Biochem.* **230**, 1014–1024 (1995).
14. I. Q. H. Phan, J. Boyd, and I. D. Campbell, Dynamic studies of a fibronectin type I module pair at three frequencies: Anisotropic

- modelling and direct determination of conformational exchange, *J. Biomol. NMR* **8**, 369–378 (1996).
15. G. Lipari and A. Szabo, Model-free approach to the interpretation of nuclear magnetic resonance relaxation in macromolecules. 1. Theory and range of validity, *J. Am. Chem. Soc.* **104**, 4546–4559 (1982).
 16. R. Brüschweiler, X. Liao, and P. E. Wright, Long-range motional restrictions in a multidomain zinc-finger protein from anisotropic tumbling, *Science* **268**, 886–889 (1995).
 17. L. K. Lee, M. Rance, W. J. Chazin, and A. G. Palmer III, Rotational diffusion anisotropy of proteins from simultaneous analysis of ^{15}N and $^{13}\text{C}\alpha$ nuclear spin relaxation, *J. Biomol. NMR* **9**, 287–298 (1997).
 18. D. S. Sivia, "Data Analysis: A Bayesian Tutorial," Oxford Univ. Press, Oxford (1996).
 19. D. E. Woessner, Nuclear spin relaxation in ellipsoids undergoing rotational Brownian motion, *J. Chem. Phys.* **37**, 647–654 (1962).
 20. A. Abragam, "Principles of Nuclear Magnetism," Oxford Univ. Press, Oxford (1961).
 21. D. Fushman, N. Tjandra, and D. Cowburn, Direct measurement of ^{15}N chemical shift anisotropy in solution, *J. Am. Chem. Soc.* **120**, 10947–10952 (1998).
 22. J. Boyd and C. Redfield, Defining the orientation of the ^{15}N shielding tensor using ^{15}N relaxation data for a protein in solution, *J. Am. Chem. Soc.* **120**, 9692–9693 (1998).
 23. C. Scheurer, N. R. Skrynnikov, S. F. Lienin, S. K. Straus, R. Brüschweiler, and R. R. Ernst, Effects of dynamics and environment on ^{15}N chemical shielding anisotropy in proteins: A combination of density functional theory, molecular dynamics simulation, and NMR relaxation, *J. Am. Chem. Soc.* **121**, 4242–4251 (1999).
 24. M. Blackledge, F. Cordier, P. Dosset, and D. Marion, Precision and uncertainty in the characterization of anisotropic rotational diffusion by ^{15}N relaxation, *J. Am. Chem. Soc.* **120**, 4538–4539 (1998).
 25. M. J. Schervish, "Theory of Statistics," Springer-Verlag, New York (1995).
 26. R. E. Kass and A. E. Raftery, Bayes factors, *J. Am. Stat. Assoc.* **90**, 773–795 (1995).
 27. I. Verdinelli and L. Wasserman, Computing Bayes factors using a generalization of the Savage–Dickey density ratio, *J. Am. Stat. Assoc.* **90**, 614–618 (1995).
 28. P. R. Bevington, "Data Reduction and Error Analysis in the Physical Sciences," McGraw–Hill, New York (1969).
 29. S. Wolfram, "The Mathematica Book," Wolfram Media/Cambridge Univ. Press, Champaign, IL (1996).
 30. B. W. Schäfer and C. W. Heizmann, The S100 family of EF-hand calcium-binding proteins: Functions and pathology, *TIBS* **21**, 134–140 (1996).
 31. A. C. Drohat, J. C. Amburgey, F. Abildgaard, M. R. Starich, D. Baldisseri, and D. J. Weber, Solution structure of rat Apo-S100B($\beta\beta$) as determined by NMR spectroscopy, *Biochemistry* **35**, 11577–11588 (1996).
 32. A. C. Drohat, N. Tjandra, D. M. Baldisseri, and D. J. Weber, The use of dipolar couplings for determining the solution structure of rat apo-S100B($\beta\beta$), *Protein Sci.* **8**, 800–809 (1999).
 33. A. M. Mandel, M. Akke, and A. G. Palmer III, Backbone dynamics of *Escherichia coli* ribonuclease HI: Correlations with structure and function in an active enzyme, *J. Mol. Biol.* **246**, 144–163 (1995).
 34. K. Pervushin, R. Riek, G. Wider, and K. Wüthrich, Attenuated T_2 relaxation by mutual cancellation of dipole–dipole coupling and chemical shift anisotropy indicates an avenue to NMR structures of very large biological macromolecules in solution, *Proc. Natl. Acad. Sci. USA* **94**, 12366–12371 (1997).
 35. D. Fushman and D. Cowburn, The effect of noncollinearity of ^{15}N – ^1H dipolar and ^{15}N CSA tensors and rotational anisotropy on ^{15}N relaxation, CSA/dipolar cross correlation, and TROSY, *J. Biomol. NMR* **13**, 139–147 (1999).
 36. A. Papoulis, "Probability, Random Variables, and Stochastic Processes," McGraw–Hill, New York (1965).
 37. W. R. Gilks, S. Richardson, and D. J. Spiegelhalter (Eds.), "Markov Chain Monte Carlo in Practice," Chapman & Hall, London (1996).
 38. N. Metropolis, A. W. Rosenbluth, M. N. Rosenbluth, A. H. Teller, and E. Teller, Equation of state calculations by fast computing machine, *J. Chem. Phys.* **21**, 1087–1091 (1953).
 39. D. Jin, F. Figueirido, G. T. Montelione, and R. M. Levy, Impact of the precision in NMR relaxation measurements on the interpretation of protein dynamics, *J. Am. Chem. Soc.* **119**, 6923–6924 (1997).
 40. D. Jin, M. Andrec, G. T. Montelione, and R. M. Levy, Propagation of experimental uncertainties using the Lipari–Szabo model-free analysis of protein dynamics, *J. Biomol. NMR* **12**, 471–492 (1998).
 41. R. M. Neal, "Markov Chain Monte Carlo Methods Based on 'Slicing' the Density Function," Technical Report 9722, Department of Statistics, University of Toronto (1997).
 42. A. J. Izenman, Recent developments in nonparametric density estimation, *J. Am. Stat. Assoc.* **86**, 205–224 (1991).
 43. G. R. Terrell, The maximal smoothing principle in density estimation, *J. Am. Stat. Assoc.* **85**, 470–477 (1990).
 44. W. H. Press, S. A. Teukolsky, W. T. Vetterling, and B. P. Flannery, "Numerical Recipes in C: The Art of Scientific Computing," Cambridge Univ. Press, Cambridge (1992).